

The strong first order electroweak phase transition in the $U(1)_X$ SSM

Shu-Min Zhao^{1,2*}, Jian-Fei Zhang^{1,2†}, Xing-Xing Dong^{1,2‡}, Tai-Fu Feng^{1,2,3§}

¹ *Department of Physics, Hebei University, Baoding 071002, China*

² *Key Laboratory of High-precision Computation and Application of Quantum Field Theory of Hebei Province, Baoding 071002, China and*

³ *Department of Physics, Chongqing University, Chongqing 401331, China*

(Dated: September 17, 2021)

Abstract

In the $U(1)_X$ extension of the minimal supersymmetric standard model, we study a two step phase transition for the universe. The first step happens at high temperature from origin to z coordinate axis. The second step is the electroweak phase transition(EWPT) with barrier between two minima, which is the first order EWPT. We study the condition for this type phase transition to occur. The strong first order EWPT is our expectation, and with the supposed parameters the evolution of the universe is plotted by the figures.

PACS numbers:

Keywords: supersymmetry, electroweak phase transition, first order

* zhaosm@hbu.edu.cn

† zjf09@hbu.edu.cn

‡ dxx_0304@163.com

§ fengtf@hbu.edu.cn

I. INTRODUCTION

Though the standard model(SM) has achieved great success for an excellent description of many experiment data in particle physics, it still fails to explain some puzzles: 1 It can not produce tiny mass to light neutrino[1]; 2 It can not provide a cold dark matter candidate; 3 The observed baryon asymmetry of the universe (BAU) is not explained in the SM[2]. On the supposition that the BAU is generated via the electroweak baryogenesis[3, 4], the strong first order electroweak phase transition(EWPT) is necessary to provide a non-equilibrium environment[5, 6]. If the Higgs mass is less than 45 GeV, the strong EWPT can take place in the SM. However, it conflicts with the present experiment data for the lightest CP-even Higgs mass $m_{h^0} = 125$ GeV. The SM CP-violation in the CKM matrix is so small that it is not able to generate a sufficient baryon asymmetry during the EWPT[2]. To solve this problem, the extension of SM with extra Higgs, heavy fermions and supersymmetric extensions of SM are possible ways[7].

During the popular models of new physics, the minimal supersymmetric extension of the standard model(MSSM)[8] is a favorite one, which has been well studied for many years. In the MSSM, there are additional sources of CP violation: the phases of μ and supersymmetric breaking parameters. To generate a strong first order EWPT, the lightest stop quark mass should be lighter than the top quark mass $m_t \sim 173$ GeV, that is called as the light stop scenario[9]. However, the current experiment constraint for the lightest stop quark mass is $m_{\tilde{t}} > 1100$ GeV[10]. With addition of the singlet S , the next-to-minimal supersymmetric standard model(NMSSM)[11] has a trilinear term $A_h h S H_u H_d$ in the Higgs potential. In this condition, a strong enough first order EWPT is allowed to occur[12].

Taking into account the shortcomings of MSSM such as: μ problem and neutrino with zero mass, physicists extend MSSM and obtain many new supersymmetric models, where the U(1) extension is an interesting type[13]. There are some works of the strong first order EWPT in the U(1) extensions of MSSM[14]. In this work, we add three Higgs singlets η , $\bar{\eta}$, S and three generation right-handed neutrinos to the $U(1)_X$ extension of MSSM. This model is called as $U(1)_X$ SSM with the local group $SU(3)_C \otimes SU(2)_L \otimes U(1)_Y \otimes U(1)_X$ [15, 16]. The right-handed neutrinos and the added Higgs singlets produce several effects: Light neutrinos obtain tiny masses through see-saw mechanism; Right-handed neutrino possesses dark matter character; Scalar neutrino can be dark matter candidate. Comparing with

MSSM, the so called little hierarchy problem in $U(1)_X$ SSM is relived because of the added superfields.

In the superpotential of $U(1)_X$ SSM, there are two terms: $\mu\hat{H}_u\hat{H}_d$ and $\lambda_H\hat{S}\hat{H}_u\hat{H}_d$. Considering \hat{S} with a non-zero VEV ($v_S/\sqrt{2}$), an effective $\mu_{eff} = \mu + \lambda_H v_S/\sqrt{2}$ is obtained. So, it can relieve the μ problem. In the soft breaking terms, there are $B_S S^2$, $L_S S$, $\frac{T_\kappa}{3} S^3$, $T_{\lambda_C} S \eta \bar{\eta}$, $\epsilon_{ij} T_{\lambda_H} S H_d^i H_u^j$, which appear in the Higgs potential. These terms allow strong first order EWPT to take place. This model has more CP-violating sources than MSSM and can generate sufficient baryon asymmetry during EWPT.

In section 2, we introduce the main content of $U(1)_X$ SSM. The temperature corrections for the particle masses and the one loop effective potential at finite temperature are given out in section 3. We study the numerical results and plot the figures in section 4. The discussion and conclusion are shown in the last section.

II. THE $U(1)_X$ SSM

Extending the local gauge group to $SU(3)_C \otimes SU(2)_L \otimes U(1)_Y \otimes U(1)_X$ and introducing three-generation right-handed neutrinos and three Higgs singlets to MSSM, we obtain the $U(1)_X$ extension of MSSM, which is called as $U(1)_X$ SSM. The right-handed neutrinos and Higgs singlets can solve the problem of light neutrino mass and mixing. The CP-even parts of the singlets η , $\bar{\eta}$ and S mix with the corresponding parts of H_u and H_d . Then the mass squared matrix of neutral CP-even Higgs is extended to 5×5 . The introduction of S can improve the lightest CP even Higgs mass at tree level. One can find the particle contents in our previous work[15].

For $U(1)_X$ SSM, the superpotential reads as

$$\begin{aligned}
W = & l_W \hat{S} + \mu \hat{H}_u \hat{H}_d + M_S \hat{S} \hat{S} - Y_d \hat{d} \hat{q} \hat{H}_d - Y_e \hat{e} \hat{l} \hat{H}_d + \lambda_H \hat{S} \hat{H}_u \hat{H}_d \\
& + \lambda_C \hat{S} \hat{\eta} \hat{\eta} + \frac{\kappa}{3} \hat{S} \hat{S} \hat{S} + Y_u \hat{u} \hat{q} \hat{H}_u + Y_X \hat{\nu} \hat{\eta} \hat{\nu} + Y_\nu \hat{\nu} \hat{l} \hat{H}_u.
\end{aligned} \tag{1}$$

The two Higgs doublets are same as those in MSSM,

$$\begin{aligned}
H_d = & \begin{pmatrix} H_d^0 \\ H_d^- \end{pmatrix}, & H_u = & \begin{pmatrix} H_u^+ \\ H_u^0 \end{pmatrix}, \\
H_d^0 = & \frac{v_d + \phi_d^0 + iP_d^0}{\sqrt{2}}, & H_u^0 = & \frac{v_u + \phi_u^0 + iP_u^0}{\sqrt{2}}.
\end{aligned} \tag{2}$$

$\tan\beta = v_u/v_d$ is defined by the VEVs of the Higgs superfields H_u and H_d .

The concrete forms of three Higgs singlets read as

$$\eta = \frac{v_\eta + \phi_\eta^0 + iP_\eta^0}{\sqrt{2}}, \quad \bar{\eta} = \frac{v_{\bar{\eta}} + \phi_{\bar{\eta}}^0 + iP_{\bar{\eta}}^0}{\sqrt{2}}, \quad S = \frac{v_S + \phi_S^0 + iP_S^0}{\sqrt{2}}. \quad (3)$$

v_η , $v_{\bar{\eta}}$ and v_S are the VEVs of the Higgs superfields η , $\bar{\eta}$ and S respectively. The β_η is defined as $\tan\beta_\eta = v_{\bar{\eta}}/v_\eta$.

The soft SUSY breaking terms of this model are shown as

$$\begin{aligned} \mathcal{L}_{soft} = & \mathcal{L}_{soft}^{MSSM} - B_S S^2 - L_S S - \frac{T_\kappa}{3} S^3 - T_{\lambda_C} S \eta \bar{\eta} + \epsilon_{ij} T_{\lambda_H} S H_d^i H_u^j \\ & - T_X^{IJ} \bar{\eta} \tilde{\nu}_R^{*I} \tilde{\nu}_R^{*J} + \epsilon_{ij} T_\nu^{IJ} H_u^i \tilde{\nu}_R^{*I} \tilde{\nu}_R^{*J} - m_\eta^2 |\eta|^2 - m_{\bar{\eta}}^2 |\bar{\eta}|^2 \\ & - m_S^2 S^2 - (m_{\tilde{\nu}_R}^2)^{IJ} \tilde{\nu}_R^{*I} \tilde{\nu}_R^{*J} - \frac{1}{2} (M_S \lambda_{\tilde{X}}^2 + 2M_{BB'} \lambda_{\tilde{B}} \lambda_{\tilde{X}}) + h.c. \end{aligned} \quad (4)$$

We use $Y^{Y(X)}$ to denote $U(1)_{Y(X)}$ charge, and the numbers of $Y^{Y(X)}$ for the superfields are given out in our previous work[15]. We have proven that $U(1)_X$ SSM is anomaly free. The gauge kinetic mixing is a new effect, which is produced by two Abelian groups $U(1)_Y$ and $U(1)_X$.

In the $U(1)_X$ SSM, the covariant derivatives can be expressed as [17]

$$D_\mu = \partial_\mu - i \begin{pmatrix} Y^Y & Y^X \end{pmatrix} \begin{pmatrix} g_Y & g'_{YX} \\ g'_{XY} & g'_X \end{pmatrix} \begin{pmatrix} A_\mu^Y \\ A_\mu^X \end{pmatrix}. \quad (5)$$

A_μ^Y and A_μ^X are the gauge fields of $U(1)_Y$ and $U(1)_X$. Because the two Abelian gauge groups are unbroken, we can rotate the gauge coupling matrix with R [17] to make one non-diagonal element zero.

$$\begin{pmatrix} g_Y & g'_{YX} \\ g'_{XY} & g'_X \end{pmatrix} R^T = \begin{pmatrix} g_1 & g_{YX} \\ 0 & g_X \end{pmatrix}. \quad (6)$$

Three gauge bosons A_μ^X , A_μ^Y and V_μ^3 mix together and produce a 3×3 mass squared matrix for neutral gauge bosons[18]. To diagonalize this matrix, two mixing angles θ_W and θ'_W are needed. $\sin^2\theta'_W$ is defined as[18]

$$\sin^2\theta'_W = \frac{1}{2} - \frac{((g_{YX} + g_X)^2 - g_1^2 - g_2^2)v^2 + 4g_X^2\xi^2}{2\sqrt{((g_{YX} + g_X)^2 + g_1^2 + g_2^2)v^4 + 8g_X^2((g_{YX} + g_X)^2 - g_1^2 - g_2^2)v^2\xi^2 + 16g_X^4\xi^4}} \quad (7)$$

The eigenvalues of the mass squared matrix for neutral gauge bosons are deduced. One is zero mass corresponding to photon. The other two values are for Z and Z'

$$m_{Z,Z'}^2 = \frac{1}{8} \left((g_1^2 + g_2^2 + (g_{YX} + g_X)^2)v^2 + 4g_X^2\xi^2 \right. \\ \left. \mp \sqrt{(g_1^2 + g_2^2 + (g_{YX} + g_X)^2)^2v^4 + 8((g_{YX} + g_X)^2 - g_1^2 - g_2^2)g_X^2v^2\xi^2 + 16g_X^4\xi^4} \right). \quad (8)$$

Here, $v = \sqrt{v_u^2 + v_d^2}$ and $\xi = \sqrt{v_\eta^2 + v_{\bar{\eta}}^2}$.

At tree level, the Higgs potential is deduced[15]

$$V_0 = \frac{1}{2}g_X(g_X + g_{YX})(|H_d^0|^2 - |H_u^0|^2)(|\eta|^2 - |\bar{\eta}|^2) + |\lambda_H|^2|H_u^0H_d^0|^2 + m_s^2|S|^2 \\ + \frac{1}{8}(g_1^2 + g_2^2 + (g_X + g_{YX})^2)(|H_d^0|^2 - |H_u^0|^2)^2 + \frac{1}{2}g_X^2(|\eta|^2 - |\bar{\eta}|^2)^2 + \lambda_C^2|\eta\bar{\eta}|^2 \\ + (|\mu|^2 + |\lambda_H|^2|S|^2 + 2\text{Re}[\mu^*\lambda_H S])(|H_d^0|^2 + |H_u^0|^2) + |\lambda_C|^2|S|^2(|\eta|^2 + |\bar{\eta}|^2) \\ + 2\text{Re}[l_W^*(2M_S S + \lambda_C\eta\bar{\eta} - \lambda_H H_u^0 H_d^0 + \kappa S^2)] + 4|M_S|^2|S|^2 + 2\text{Re}[\lambda_C^*\kappa\eta^*\bar{\eta}^*S^2] \\ + |\kappa|^2|S|^4 + 4\text{Re}[M_S^*S^*(\lambda_C\eta\bar{\eta} - \lambda_H H_u^0 H_d^0 + \kappa S^2)] - 2\text{Re}[\lambda_C^*\lambda_H\eta^*\bar{\eta}^*H_u^0H_d^0] + |l_W|^2 \\ - 2\text{Re}[B_\mu H_d^0 H_u^0] + 2\text{Re}[L_S S] + \frac{2}{3}\text{Re}[T_\kappa S^3] + 2\text{Re}[T_{\lambda_C}\eta\bar{\eta}S] - 2\text{Re}[T_{\lambda_H}H_d^0H_u^0S] \\ - 2\text{Re}[\lambda_H\kappa^*H_u^0H_d^0(S^2)^*] + m_\eta^2|\eta|^2 + m_{\bar{\eta}}^2|\bar{\eta}|^2 + m_{H_u^0}^2|H_u|^2 + m_{H_d^0}^2|H_d|^2 + 2\text{Re}[B_S S^2]. \quad (9)$$

The parameters (μ , λ_H , λ_C , l_W , M_S , B_μ , L_S , T_κ , T_{λ_C} , T_{λ_H} , κ , B_S) in Eq. (9) are supposed as real parameters to simplify the discussion. Through the formula

$$\left\langle \frac{\partial V_{tree}}{\partial H_u^0} \right\rangle = \left\langle \frac{\partial V_{tree}}{\partial H_d^0} \right\rangle = \left\langle \frac{\partial V_{tree}}{\partial \eta} \right\rangle = \left\langle \frac{\partial V_{tree}}{\partial \bar{\eta}} \right\rangle = \left\langle \frac{\partial V_{tree}}{\partial S} \right\rangle = 0, \quad (10)$$

one can obtain the following tadpole equations[15]

$$\frac{v_d^2 - v_u^2}{8}(g_1^2 + g_2^2 + (g_X + g_{YX})^2) + \frac{g_X}{4}(g_X + g_{YX})(v_\eta^2 - v_{\bar{\eta}}^2) + \mu^2 + \frac{\lambda_H^2}{2}(v_u^2 + v_S^2) + m_{H_d^0}^2 \\ + \sqrt{2}\mu\lambda_H v_S - [\lambda_H(\sqrt{2}M_S v_S + l_W + \frac{\lambda_C}{2}v_\eta v_{\bar{\eta}} + \frac{\kappa}{2}v_S^2) + B_\mu - \frac{T_{\lambda_H}}{\sqrt{2}}v_S] \tan \beta = 0, \quad (11)$$

$$\frac{v_u^2 - v_d^2}{8}(g_1^2 + g_2^2 + (g_X + g_{YX})^2) + \frac{g_X}{4}(g_X + g_{YX})(v_\eta^2 - v_{\bar{\eta}}^2) + \mu^2 + \frac{\lambda_H^2}{2}(v_S^2 + v_d^2) + m_{H_u^0}^2 \\ + \sqrt{2}\mu\lambda_H v_S - [\lambda_H(\sqrt{2}M_S v_S + l_W + \frac{\lambda_C}{2}v_\eta v_{\bar{\eta}} + \frac{\kappa}{2}v_S^2) + B_\mu + \frac{T_{\lambda_H}}{\sqrt{2}}v_S] \cot \beta = 0, \quad (12)$$

$$\frac{g_X^2}{2}(v_\eta^2 - v_{\bar{\eta}}^2) - \frac{g_X}{4}(g_X + g_{YX})(v_u^2 - v_d^2) + \frac{\lambda_C^2}{2}(v_S^2 + v_{\bar{\eta}}^2) + m_\eta^2 + [\lambda_C(l_W + \sqrt{2}M_S v_S \\ - \frac{1}{2}\lambda_H v_u v_d + \frac{1}{2}\kappa v_S^2) + \frac{T_{\lambda_H}}{\sqrt{2}}v_S] \tan \beta_\eta = 0, \quad (13)$$

$$\frac{1}{2}g_X^2(v_\eta^2 - v_{\bar{\eta}}^2) + \frac{1}{4}g_X(g_X + g_{YX})(v_u^2 - v_d^2) + \frac{1}{2}\lambda_C^2(v_S^2 + v_\eta^2) + m_{\bar{\eta}}^2 + [\lambda_C(l_W + \sqrt{2}M_S v_S$$

$$-\frac{1}{2}\lambda_H v_u v_d + \frac{1}{2}\kappa v_S^2) + \frac{T\lambda_H}{\sqrt{2}}v_S] \cot \beta_\eta = 0, \quad (14)$$

$$\begin{aligned} & \frac{\lambda_H^2}{2}v^2 + \frac{\lambda_C^2}{2}\xi^2 + 4M_S^2 + \kappa(\kappa v_S^2 + 2l_W + 3\sqrt{2}M_S v_S + \lambda_C v_\eta v_{\bar{\eta}} - \lambda_H v_u v_d) + \frac{T\kappa v_S}{\sqrt{2}} + 2B_S \\ & + m_S^2 + [L_S + M_S(2l_W + \lambda_C v_\eta v_{\bar{\eta}} - \lambda_H v_u v_d) + \frac{\mu\lambda_H v^2 + T\lambda_C v_\eta v_{\bar{\eta}} - T\lambda_H v_u v_d}{2}] \frac{\sqrt{2}}{v_S} = 0. \end{aligned} \quad (15)$$

III. THE ONE LOOP EFFECTIVE POTENTIAL AT FINITE TEMPERATURE

To simplify the discussion, we change the tree level potential V_0 in Eq.(9) to the form $V_0(h, y, z)$ with the relations

$$\begin{aligned} h^2 &= (\phi_d^0)^2 + (\phi_u^0)^2, & y^2 &= (\phi_\eta^0)^2 + (\phi_{\bar{\eta}}^0)^2, \\ z^2 &= (\phi_S^0)^2, & \frac{\phi_u^0}{\phi_d^0} &= \tan \beta, & \frac{\phi_{\bar{\eta}}^0}{\phi_\eta^0} &= \tan \beta_\eta. \end{aligned} \quad (16)$$

The one loop effective potential at finite temperature[19] can be written in the following form[7]

$$V_{eff}(h, y, z, T) = V_0(h, y, z) + V_1(h, y, z, 0) + \Delta V_1(h, y, z, T) + \Delta V_{daisy}(h, y, z, T). \quad (17)$$

Here, $V_0(h, y, z)$ is the tree level potential. The one loop zero temperature correction is represented by $V_1(h, y, z, 0)$ [20]. $\Delta V_1(h, y, z, T)$ represents the temperature dependent one loop correction[21], while $\Delta V_{daisy}(h, y, z, T)$ denotes the multi-loop daisy correction[22].

The concrete forms of $V_1(h, y, z, 0)$, $\Delta V_1(h, y, z, T)$ and $\Delta V_{daisy}(h, y, z, T)$ are shown explicitly

$$\begin{aligned} V_1(h, y, z, 0) &= \sum_i \frac{n_i}{64\pi^2} m_i^4(h, y, z) \left(\log \frac{m_i^2(h, y, z)}{Q^2} - C_i \right), \\ V_1(h, y, z, T) &= \frac{T^4}{2\pi^2} \left\{ \sum_i n_i J_i \left[\frac{m_i^2(h, y, z)}{T^2} \right] \right\}, \\ \Delta V_{daisy}(h, y, z, T) &= -\frac{T}{12\pi} \sum_{i=\text{bosons}} n_i [\mathcal{M}_i^3(h, y, z, T) - m_i^3(h, y, z)], \end{aligned} \quad (18)$$

with $m_i(h, y, z)$ denoting field-dependent masses and n_i being the number of degrees of freedom. The contents C_i depend on the regularization scheme. In the \overline{MS} scheme, they are assumed as $C_i = \frac{3}{2}$ for scalars and fermions and $C_i = \frac{5}{6}$ for gauge bosons. For bosons and fermions, the J_i functions in the one loop effective potential at finite temperature have

different forms[7, 23]

$$\begin{aligned} J_B[m_B^2(h, y, z)/T^2] &= \int_0^\infty dx x^2 \log \left\{ 1 - \exp \left[-\sqrt{x^2 + m_B^2(h, y, z)/T^2} \right] \right\}, \\ J_F[m_F^2(h, y, z)/T^2] &= \int_0^\infty dx x^2 \log \left\{ 1 + \exp \left[-\sqrt{x^2 + m_F^2(h, y, z)/T^2} \right] \right\}. \end{aligned} \quad (19)$$

At high temperature and low temperature, the functions $J_B[m_B^2(h, y, z)/T^2]$ and $J_F[m_F^2(h, y, z)/T^2]$ can be expanded. In the numerical calculation of Ref.[7], the authors give perfect approximations for the functions $J_B[m_B^2(h, y, z)/T^2]$ and $J_F[m_F^2(h, y, z)/T^2]$.

Adding temperature dependent self-energy contributions $\Pi(T)$ to $m_i^2(h, y, z)$, one can obtain the temperature dependent scalar mass squared $\mathcal{M}^2(h, y, z, T) = m^2(h, y, z) + \Pi(T)$ [24]. In this equation, $\Pi(T)$ is proportional to T^2 . The longitudinal components of gauge bosons receive such contributions. The $\Pi(T)$ for particles in $U(1)_X$ SSM are shown here.

1. $\Pi(T)$ for scalar quarks

$$\begin{aligned} \Pi_{\tilde{Q}_i}(T) &= \left(\frac{2}{3}g_3^2 + \frac{3}{8}g_2^2 + \frac{1}{72}g_1^2 + \frac{1}{4}(Y_{u_i}^2 + Y_{d_i}^2) \right) T^2, \\ \Pi_{\tilde{u}_R^i}(T) &= \left(\frac{2}{3}g_3^2 + \frac{2}{9}g_1^2 + \frac{1}{2}Y_{u_i}^2 + \frac{1}{8}g_X^2 \right) T^2, \\ \Pi_{\tilde{d}_R^i}(T) &= \left(\frac{2}{3}g_3^2 + \frac{1}{18}g_1^2 + \frac{1}{2}Y_{d_i}^2 + \frac{1}{8}g_X^2 \right) T^2. \end{aligned} \quad (20)$$

2. $\Pi(T)$ for scalar charged leptons and scalar neutrinos

$$\begin{aligned} \Pi_{\tilde{L}_i}(T) &= \left(\frac{3}{8}g_2^2 + \frac{1}{8}g_1^2 + \frac{1}{4}Y_{e_i}^2 \right) T^2, \quad \Pi_{\tilde{e}_R^i}(T) = \left(\frac{1}{2}g_1^2 + \frac{1}{2}Y_{e_i}^2 + \frac{1}{8}g_X^2 \right) T^2, \\ \Pi_{\tilde{\nu}_R^i}(T) &= \left(\frac{1}{4}Y_X^2 + \frac{1}{8}g_X^2 \right) T^2. \end{aligned} \quad (21)$$

3. $\Pi(T)$ for Higgs doublets and singlets

$$\begin{aligned} \Pi_{H_d}(T) &= \left(\frac{3}{8}g_2^2 + \frac{1}{8}g_1^2 + \frac{3}{4}Y_b^2 + \frac{1}{8}g_X^2 + \frac{1}{4}Y_{e_3}^2 + \frac{1}{4}\lambda_H^2 \right) T^2, \\ \Pi_{H_u}(T) &= \left(\frac{3}{8}g_2^2 + \frac{1}{8}g_1^2 + \frac{3}{4}Y_t^2 + \frac{1}{8}g_X^2 + \frac{1}{4}\lambda_H^2 \right) T^2, \quad \Pi_\eta(T) = \left(\frac{1}{2}g_X^2 + \frac{1}{4}\lambda_C^2 \right) T^2, \\ \Pi_{\bar{\eta}}(T) &= \left(\frac{1}{2}g_X^2 + \frac{1}{4}\lambda_C^2 + \frac{1}{4}\lambda_X^2 \right) T^2, \quad \Pi_S(T) = \left(\frac{1}{4}\kappa^2 + \frac{1}{4}\lambda_C^2 + \frac{1}{2}\lambda_H^2 \right) T^2. \end{aligned} \quad (22)$$

4. $\Pi(T)$ for the longitudinal components of gauge bosons

$$\begin{aligned} \Pi_{g_3}(T) &= \frac{9}{2}g_3^2 T^2, & \Pi_{g_2}(T) &= \frac{9}{2}g_2^2 T^2, \\ \Pi_{g_1}(T) &= \frac{11}{2}g_1^2 T^2, & \Pi_{g_X}(T) &= \frac{9}{2}g_X^2 T^2. \end{aligned} \quad (23)$$

At finite temperature, the effective potential receives the thermal corrections. We keep only the leading T^2 terms and show the finite temperature effective potential as

$$V_{eff}(h, y, z, T) = \frac{L_h}{4}h^4 + \frac{L_{hy}}{2}h^2y^2 + \frac{M_h^2}{2}h^2 + \frac{L_y}{4}y^4 + \frac{M_y^2}{2}y^2 + \frac{L_{hz}}{2}h^2z^2 + \frac{L_{yz}}{2}y^2z^2 + \frac{L_z}{4}z^4 + \frac{M_z^2}{2}z^2 + \left(\frac{B_{ht}}{2}h^2 + \frac{B_{\eta t}}{2}y^2 + \frac{B_{st}}{2}z^2\right)T^2 + R_{hs}h^2z + R_{\eta s}y^2z + R_{ss}z^3 + N_s z. \quad (24)$$

The concrete forms of the coefficients L_h , L_y , L_z ... are collected here

$$\begin{aligned} L_h &= \frac{g_1^2 + g_2^2 + g_X^2}{8} \cos^2 2\beta + \frac{\lambda_H^2}{4} \sin^2 2\beta, & L_y &= \frac{g_X^2}{2} \cos^2 2\beta_\eta + \frac{\lambda_C^2}{4} \sin^2 2\beta_\eta, \\ L_{hy} &= \frac{g_X^2}{4} \cos 2\beta \cos 2\beta_\eta + \frac{\lambda_C \lambda_H}{4} \sin 2\beta \sin 2\beta_\eta, & L_z &= \kappa^2, \\ L_{hz} &= \frac{\lambda_H \kappa}{2} \sin 2\beta + \frac{\lambda_H^2}{2}, & L_{yz} &= \frac{\kappa \lambda_C}{2} \sin(2\beta_\eta) + \frac{\lambda_C^2}{2}. \end{aligned} \quad (25)$$

M_h^2 , M_y^2 and M_z^2 read as

$$\begin{aligned} M_h^2 &= \sin(2\beta)[\lambda_H(l_W + \sqrt{2}M_S) - B_\mu] + m_{H_d}^2 \cos^2 \beta + m_{H_u}^2 \sin^2 \beta + \mu^2, \\ M_y^2 &= \lambda_C l_W \sin 2\beta_\eta + m_\eta^2 \cos^2 \beta_\eta + m_{\bar{\eta}}^2 \sin^2 \beta_\eta, & M_z^2 &= 2B_S + 2\kappa l_W + m_s^2 + 4M_S^2. \end{aligned} \quad (26)$$

The parameters with odd-order unit of mass are R_{hs} , $R_{\eta s}$, R_{ss} and N_s

$$\begin{aligned} R_{hs} &= \frac{\lambda_H \mu}{\sqrt{2}} - \frac{T \lambda_H \sin 2\beta}{2\sqrt{2}}, & R_{\eta s} &= \left(\frac{\lambda_C M_S}{\sqrt{2}} + \frac{T \lambda_C}{2\sqrt{2}}\right) \sin 2\beta_\eta, \\ R_{ss} &= \sqrt{2} \kappa M_S + \frac{T \kappa}{3\sqrt{2}}, & N_s &= \sqrt{2} L_{lw} + 2\sqrt{2} l_W M_S. \end{aligned} \quad (27)$$

The terms B_{ht} , $B_{\eta t}$ and B_{st} have relation with temperature correction and are all positive

$$\begin{aligned} B_{ht} &= \frac{1}{8}(6Y_t^2 \sin^2 \beta + g_1^2 + 3g_2^2 + g_X^2 + 2\lambda_H^2), \\ B_{\eta t} &= \frac{1}{4}(\lambda_X^2 \sin^2 \beta_\eta + 2g_X^2 + \lambda_C^2), & B_{st} &= \frac{1}{4}(\kappa^2 + \lambda_C^2 + \lambda_H^2). \end{aligned} \quad (28)$$

If the Higgs potential does not contain tree level cubic term, the one step phase transition may take place. The loop corrections always produce the barrier between the electroweak symmetric and broken phases. For the two step phase transition, the barrier can be produced from tree level potential.

IV. NUMERICAL RESULTS

Considering our previous works in the $U(1)_X$ SSM[15], we study the numerical results in this section. The mass of the new neutral gauge boson is strict, and we take $M_{Z'} >$

4.5 TeV[15]. It is at 99% CL, that $\frac{M_{Z'}}{g_X} \geq 6\text{TeV}$ [25] for the ratio between $M_{Z'}$ and its gauge coupling. LHC experiment gives constraint for the new angle β_η as $\tan \beta_\eta < 1.5$ [26]. As a concrete example, we take the following parameters as

$$\begin{aligned} g_X &= 0.5, \quad \tan \beta = 10, \quad \tan \beta_\eta = 1.38, \quad \lambda_H = 0.5, \quad \lambda_C = 0.3, \quad \lambda_X = 2.5, \quad B_\mu = 1 \text{ TeV}^2, \\ m_s &= 1.8 \text{ TeV}, \quad T_{\lambda_C} = -1923 \text{ GeV}, \quad M_S = 3 \text{ TeV}, \quad T_\kappa = -14.4 \text{ TeV}, \quad B_S = -17 \text{ TeV}^2, \\ \mu &= -380 \text{ GeV}, \quad T_{\lambda_H} = -2 \text{ TeV}, \quad l_W = -45.21 \text{ TeV}^2, \quad L_{lw} = 271.26 \text{ TeV}^3, \quad \kappa = 0.8. \end{aligned} \quad (29)$$

The parameters $m_{H_u}^2$, $m_{H_d}^2$, m_η^2 , $m_\eta'^2$ can be calculated from the tadpole equations[15].

In our case, we suppose two step phase transition[27] considering the complex structure of the effective potential at finite temperature, which only retains the leading terms in the high T expansion. It is shown in Eq.(24) and can avoid problems relating to the gauge dependence. The desired patten of EWPT is shown in the Fig.1, where one can see the universe phase evolution with the dropping temperature. At very high temperature (larger than T_S), the point $(0, 0, 0)$ corresponds to the global minimum, and the electroweak symmetry is kept. A minimum appears in the $(0, 0, z)$ direction, when temperature drops to T_S . There is not any barrier between $V_{eff}(0, 0, z_S, T_S)$ and $V_{eff}(0, 0, 0, T_S)$. Through a second order phase transition, the universe transits to the minimum $V_{eff}(0, 0, z_S, T_S)$. As the temperature drops further to T_h , there appears another minimum $V_{eff}(0, y_h, z_h, T_h)$ in the $(0, y, z)$ plane. At the temperature T_h , the emerged minimum is higher than the one in z direction as $V_{eff}(0, y_h, z_h, T_h) > V_{eff}(0, 0, z'_h, T_h)$. When the temperature further decreases, the $V_{eff}(h, y, z, T)$ declines faster than $V_{eff}(0, 0, z, T)$. The both minima are equal at the critical temperature T_C . With T dropping slightly below T_C , the global minimum is $V_{eff}(h, y, z, T)$, to which the universe makes a second transition. This transition can be a first order EWPT, because there is the barrier between the two minima. It is caused by the tunneling process. Through nucleations of electroweak bubbles which expand, collide and coalesce, the transition proceeds and in the end the universe turns into electroweak phase. Here, electroweak baryogenesis is assumed to generate baryon asymmetry through the first order EWPT. The sphaleron process in the bubble should be sufficiently suppressed so as to preserve the generated baryon asymmetry after the EWPT. This requirement can be expressed as [7]

$$\frac{v(T_C)}{T_C} \gtrsim 1. \quad (30)$$

In the SM, $v(T)$ represents the vacuum expectation value of the Higgs field H^0 at temperature T . In the MSSM, the condition is similar

$$v(T) = \sqrt{v_d^2(T) + v_u^2(T)}. \quad (31)$$

Here, $v_d(T)$ and $v_u(T)$ are the VEVs of the two neutral Higgs H_d^0 and H_u^0 . $v(T)$ in $U(1)_X$ SSM is same as that in MSSM. From the concrete form in Eq.(24), the finite temperature effective potential possesses the reflection symmetry $h \rightarrow -h$ and $y \rightarrow -y$. Because of the odd-order terms h^2z , y^2z , z^3 and z , it does not have the reflection symmetry under $z \rightarrow -z$.

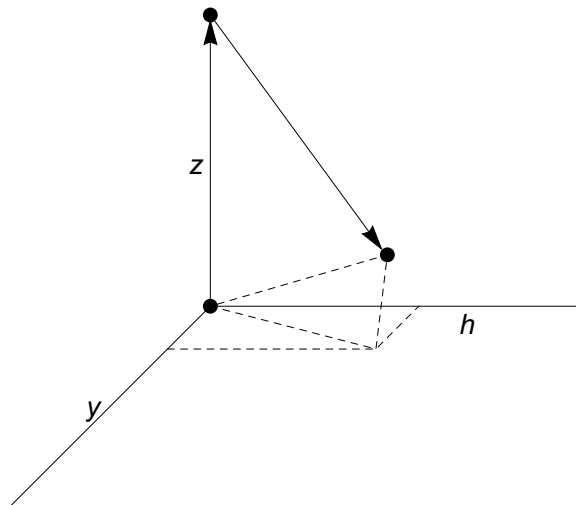


FIG. 1: This figure illustrates the picture of two step EWPT. The first step is in the $(0, 0, z)$ direction, and the second step is from z direction to the (h, y, z) direction.

With the parameters shown in Eq.(29), we plot the numerical results by the figures. The left diagram in Fig.2 shows the evolution of V_{eff} at the two minima with the temperature dropping from right to left. The dashed line represents the minimum in the $(0, 0, z)$ direction. While, the solid line denotes the minimum in the (h, y, z) direction, and it eventually evolves to the electroweak minimum at the temperature $T = 0$, which is the global minimum at the coordinate $(250 \text{ GeV}, 20795 \text{ GeV}, 2743.4 \text{ GeV})$. At the temperature $T_h = 87.3 \text{ TeV}$, a new minimum represented by Q appears at the point $(0, y, z)$. As the temperature further drops, the value of h turns larger and the solid line degenerates faster than the dashed line. The solid line and the dashed line intersect at the point P with the critical temperature $T_C = 80.3 \text{ GeV}$. The coordinates of the solid line and dashed line at T_C are $(98.7\text{GeV}, 20781.9\text{GeV}, 2758.1\text{GeV})$ and $(0, 0, 10239.2\text{GeV})$ respectively. In this condition,

$\frac{v(T_C)}{T_C} = 1.23 > 1$ can satisfy the strong first order EWPT criterion. To show the evolution of the minimum in the direction $(0, 0, z)$ at high temperature, we plot the right diagram in the Fig.2. The minimum in the direction $(0, 0, z)$ denoted by the dashed line emerges at high temperature $T_S = 16549$ GeV.

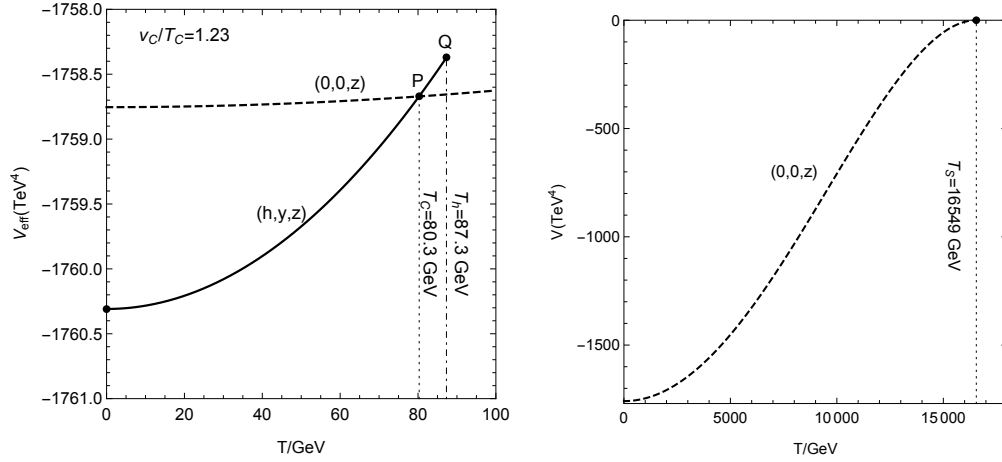


FIG. 2: The left diagram shows the evolution of V_{eff} at the two minima in $(0, 0, z)$ (dashed) and in (h, y, z) (solid) directions as T drops from right to left. The right diagram shows the evolution of V_{eff} at the minimum in the $(0, 0, z)$ direction as T drops from T_S to 0. The three characteristic temperatures from left to right are $T_C = 80.3$ GeV, $T_h = 87.3$ GeV and $T_S = 16549$ GeV respectively.

To explain the evolution of the effective potential near the temperature T_S , we plot three diagrams in the Fig.3. T_S is much higher than T_C , so we take $h = 0$. The numerical results are shown in the plane of y and z . The left diagram is plotted at $T = 21$ TeV larger than T_S , from which one can find the global minimum is the point O with coordinate $(0, 0, 0)$. At the temperature $T_S = 16.55$ TeV, the phase transition takes place and it is reflected by the middle diagram. There is no barrier between $V_{eff}(0, 0, 0, T_S)$ and $V_{eff}(0, 0, z_S, T_S)$, so it is a second order phase transition. The right diagram is plotted at the temperature $T = 15$ TeV smaller than T_S . In this condition, the global minimum has translated from O to A . Here we just discuss the situation with $z \geq 0$. When the high temperature is smaller than T_S , the point A is the global minimum.

To show the EWPT picture more explicitly, in the Fig.4 we give out the equipotential diagram at the critical temperature $T_C = 80.3$ TeV in the plane of y and z with $h = 0$. The point J appears at the temperature T_h larger than T_C . At T_h , the point J is higher than the point G . However, J point degenerates faster than G point. Then at the critical

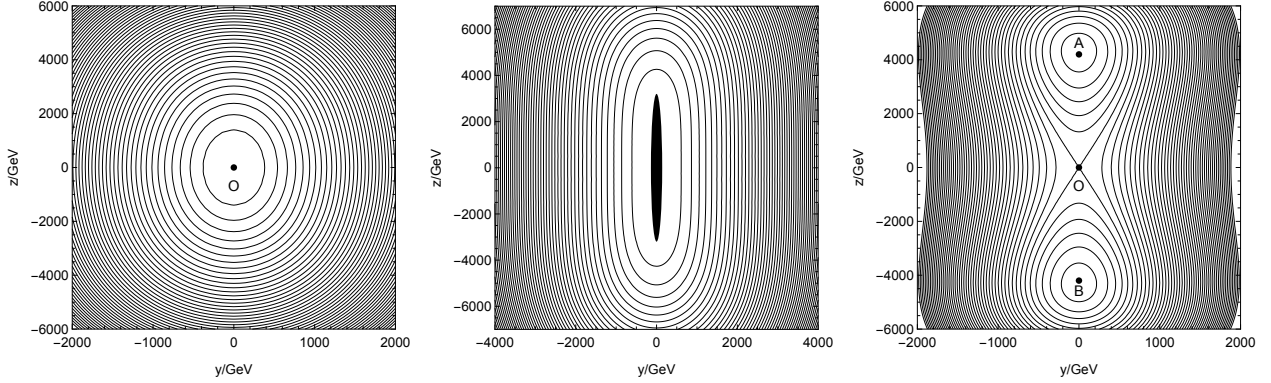


FIG. 3: These diagrams are all plotted in the plane of y and z with $h=0$. The left diagram denotes the potential at the temperature $T = 21$ TeV larger than T_S . The middle diagram denotes the potential at the temperature $T_S=16.55$ TeV. The right diagram denotes the potential at the temperature $T = 15$ TeV smaller than T_S .

temperature T_C , the two minima points G and J are equal. Thus, the first order EWPT takes place. After that, the minimum translates from G point to J point along the path denoted by the dashed line. As the temperature further drops, the point J becomes the global minimum.

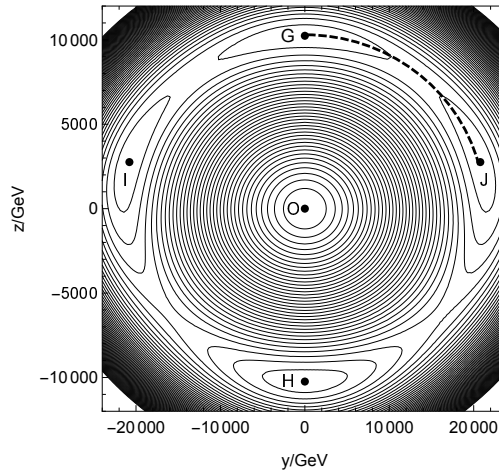


FIG. 4: At the temperature $T_C=80.3$ GeV, the effective potential is plotted in the plane of y and z with $h=98.7$ GeV and $\frac{v_C}{T_C} = 1.23$.

At the temperature $T = 0$, we show the results in the Fig.5. With $h = 250$ GeV, the potential is plotted in the plane of y and z by the left diagram. The global minimum is denoted by the point D , whose coordinate is (250 GeV, 20795 GeV, 2743.4 GeV). The right

diagram shows the potential in the plane of h and z , as $y = 20795$ GeV. It is obviously that, the point F is the global minimum and the corresponding h is equal to 250 GeV. This result satisfies our expectation.

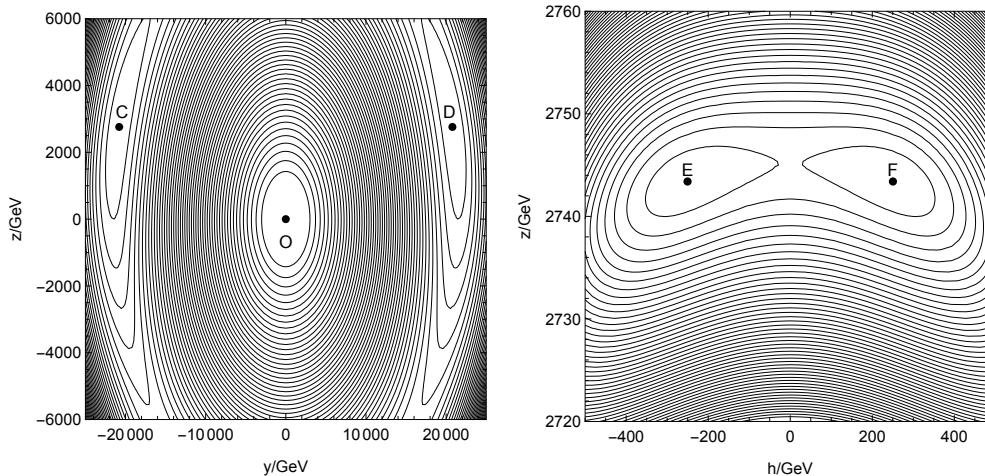


FIG. 5: At the temperature $T = 0$, we plot the effective potential. The left diagram represents the potential in the plane of y and z with $h=250$ GeV. The right diagram represents the potential in the plane of h and z with $y=20795.5$ GeV.

As shown in the Fig.2, the local minimum denoted by the point Q emerges at the temperature T_h . The coordinate(h, y, z) of this minimum is the function of temperature. To see the temperature effects on the coordinate(h, y, z), we plot h, y and z versus temperature in the Fig.6. In the left diagram, h is the decreasing function with the increasing T . As $T = T_h = 87.3$ GeV, h turns to zero. At $T = 0$, h is equal to 250 GeV. In the middle diagram, y is also the decreasing function of T , and the downward trend is gentle. In the whole, y is around 20790 GeV. As shown in the right diagram, z turns large slowly with the increasing T . The value of z varies from 2743.4 GeV to 2762 GeV in the temperature region (0, 90) GeV.

V. DISCUSSION AND CONCLUSION

In the $U(1)_X$ extension of MSSM, we study the strong first order EWPT. The Higgs singlets $\hat{\eta}$, $\hat{\bar{\eta}}$ and \hat{S} are beyond MSSM, and they bring new terms to the Higgs potential. The one loop effective potential at finite temperature is composed of four parts: the tree level potential $V_0(h, y, z)$, the one loop zero temperature correction $V_1(h, y, z, 0)$, the tem-

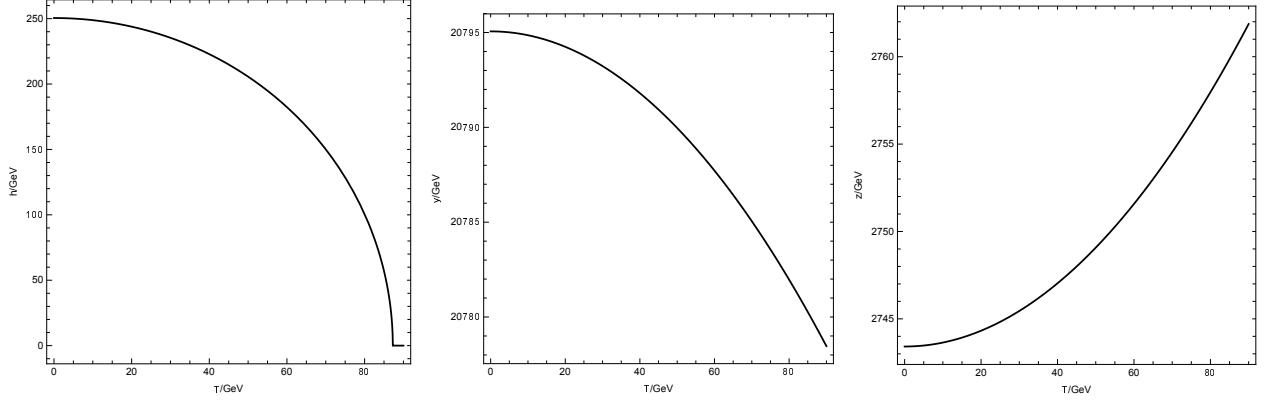


FIG. 6: When the temperature is smaller than T_C , the global minimum of the effective potential $V_{eff}(h, y, z, T)$ appears. With T varying from 0 to 90 GeV, the corresponding coordinates (h, y, z) are plotted by the left middle and right diagrams respectively.

perature dependent one loop correction $\Delta V_1(h, y, z, T)$ and the multi-loop daisy correction $\Delta V_{daisy}(h, y, z, T)$. The tree level potential has $T_{\lambda_C} S \eta \bar{\eta}$, $\epsilon_{ij} T_{\lambda_H} S H_d^i H_u^j$ etc. coming from the soft breaking terms. These terms go beyond the MSSM and allow the strong first order EWPT to take place.

In the numerical calculation, we take the parameters considering the experiment constraints. The evolution of the universe with the dropping temperature is described by the diagrams. At very high temperature, the global minimum is at the origin. As the temperature drops to T_S , a minimum appears in the $(0, 0, z)$ direction. This phase transition is the first step and belongs to the second order, because there is no barrier between $(0, 0, z)$ and origin. When the temperature drops to T_h , another minimum at (h, y, z) emerges, which is higher than the minimum in the $(0, 0, z)$ direction. This new minimum drops faster than the others as the temperature further drops. The two minima $V_{eff}(h_C, y_C, z_C, T_C)$ and $V_{eff}(0, 0, z'_C, T_C)$ are equal at the critical temperature T_C . After that, the first order EWPT occurs with the barrier between the two minima. In our numerical results, the criterion is satisfied as $\frac{v(T_C)}{T_C} \gtrsim 1$. So this step phase transition is the strong first order EWPT. In the end, the universe undergoes two step phase transitions to the real world.

Acknowledgments

This work is supported by National Natural Science Foundation of China (NNSFC) (No. 12075074), Natural Science Foundation of Hebei Province (A2020201002), and the youth top-notch talent support program of the Hebei Province.

-
- [1] T2K Collab., *Phys. Rev. Lett.* **107** (2011) 041801; MINOS Collab., *Phys. Rev. Lett.* **107** (2011) 181802; DAYA-BAY Collab., *Phys. Rev. Lett.* **108** (2012) 171803.
 - [2] A.I. Bochkarev, M.E. Shaposhnikov, *Mod. Phys. Lett. A* **2** (1987) 417; K. Kajantie, M. Laine, K. Rummukainen, et al., *Nucl. Phys. B* **466** (1996) 189 [hep-lat/9510020].
 - [3] V.A. Kuzmin, V.A. Rubakov, M.E. Shaposhnikov, *Phys. Lett. B* **155** (1985) 36; D.E. Morrissey, M.J.R. Musolf, *New J. Phys.* **14** (2012) 125003 [arXiv: 1206.2942].
 - [4] M.E. Shaposhnikov, *JETP Lett.* **44** (1986) 465.
 - [5] W. Chao, H.K. Guo, J. Shu, *JCAP* **09** (2017) 009.
 - [6] L.G. Bian, Y.C. Wu, K.P. Xie, *JHEP* **12** (2019) 028.
 - [7] J.H. Kang, P. Langacker, T.J. Li, et al., *JHEP* **04** (2011) 097 [arXiv: 0911. 2939].
 - [8] J. Rosiek, *Phys. Rev. D* **41** (1990) 3464 [Erratum: hep-ph/9511250]; H.P. Nilles, *Phys. Rept.* **110** (1984) 1-162; H.E. Haber, G.L. Kane, *Phys. Rept.* **117** (1985) 75-263.
 - [9] K. Funakubo, E. Senaha, *Phys. Rev. D* **79** (2009) 115024 [arXiv: 0905.2022]; S.W. Ham, S.K. OH, D. Son, *Phys. Rev. D* **71** (2005) 015001 [hep-ph/0411012].
 - [10] Particle Data Group, *Prog. Theor. Exp. Phys.* **2020** (2020) 083C01.
 - [11] U. Ellwanger, C. Hugonie, A.M. Teixeira, *Phys. Rept.* **496** (2010) 1-77 [arXiv: 0910.1785]; J. Ellis, J.F. Gunion, H.E. Haber, et al., *Phys. Rev. D* **39** (1989) 844; J.J. Cao, J. Li, Y.S. Pan, et al., *Phys. Rev. D* **99** (2019) 115033 [arXiv: 1807.03762].
 - [12] S.J. Huber, T. Konstandin, T. Prokopec, et al., *Nucl. Phys. B* **757** (2006) 172-196 [hep-ph/0606298].
 - [13] P. Bandyopadhyay, E.J. Chun, J.C. Park, *JHEP* **1106** (2011) 129 [arXiv: 1105. 1652]; G. Belanger, J.D. Silva, A. Pukhov, *JCAP* **1112** (2011) 014 [arXiv: 1110. 2414].
 - [14] A. Ahriche, S. Nasri, *Phys. Rev. D* **83** (2011) 045032 [arXiv: 1008.3106]; S.W. Ham, S.K. OH, *Phys. Rev. D* **76** (2007) 095018 [arXiv: 0708.1785].

- [15] S.M. Zhao, T.F. Feng, M.J. Zhang, et al., *JHEP* **02** (2020) 130; S.M. Zhao, G.Z. Ning, J.J. Feng, et al., *Nucl. Phys. B* **969** (2021) 115469.
- [16] F. Staub, *Comput. Phys. Commun.* **185** (2014) 1773 [arXiv: 1309.7223]; *Adv. High Energy Phys.* **2015** (2015) 840780 [arXiv: 1503.04200].
- [17] V. Barger, P.F. Perez, S. Spinner, *Phys. Rev. Lett.* **102** (2009) 181802 [arXiv: 0812.3661]; G. Belanger, J.D. Silva, H.M. Tran, *Phys. Rev. D* **95** (2017) 115017 [arXiv: 1703.03275].
- [18] S.M. Zhao, L.H. Su, X.X. Dong, et al., [arXiv: 2107.03571].
- [19] M.E. Carrington, *Phys. Rev. D* **45** (1992) 2933.
- [20] S.R. Coleman, *Phys. Rev. D* **7** (1973) 1888.
- [21] M. Quiros, Trieste, Italy, 29 June-17 July 1998 [hep-ph/9901312].
- [22] R.R. Parwani, *Phys. Rev. D* **45** (1992) 4695 [Erratum *ibid. D* **48** (1993) 5965] [hep-ph/9204216]; D.J. Gross, R.D. Pisarski, L.G. Yaffe, *Rev. Mod. Phys.* **53** (1981) 43.
- [23] D. Curtin, P. Meade, H. Ramani, *Eur. Phys. J. C* **78** (2018) 787.
- [24] D. Comelli, J.R. Espinosa, *Phys. Rev. D.* **55** (1997) 6253-6263 [hep-ph/9606438]; N. Haba, T.Yamada, *Phys. Rev. D.* **101** (2020) 075027.
- [25] G. Cacciapaglia, C. Csaki, G. Marandella, et al., *Phys. Rev. D* **74** (2006) 033011 [hep-ph/0604111]; M. Carena, A. Daleo, B.A. Dobrescu et al., *Phys. Rev. D* **70** (2004) 093009 [hep-ph/0408098].
- [26] L. Basso, *Adv. High Energy Phys.* **2015** (2015) 980687 [arXiv: 1504.05328].
- [27] S. Inoue, G. Ovanesyan, M.J.R. Musolf, *Phys. Rev. D* **93** (2016) 015013 [arXiv: 1508.05404]; V. Vaskonen, *Phys. Rev. D* **95** (2017) 123515 [arXiv: 1611.02073].